Predicting composite laminates roughness: data-driven modeling approaches using force sensor data from robotic manipulators

Huseyin Oktay Erkol[1,2†], Manuel Bailey[1,3†], Genevieve Palardy[1] and Corina Barbalata[1*]

[1*]Department of Mechanical & Industrial Engineering, Louisiana State University, Patrick F. Taylor Hall, Baton Rouge, 70803, Louisiana, USA.

[2]Department of Electrical Engineering, Bandirma Onyedi Eylul University, Engineering and Natural Science Faculty, Bandirma, 10200, Balikesir, Turkey.

[3]Department of Mechanical Engineering, Columbia University, 500 West 120th Street, New York, 10027, NY, USA.

*Corresponding author(s). E-mail(s): cbarbalata@lsu.edu;
Contributing authors: herkol@lsu.edu; mfb2172@columbia.edu; gpalardy@lsu.edu;
[†]These authors contributed equally to this work.

Abstract

The development of autonomous finishing operations in manufacturing process has the potential to decrease the costs and increase the quality of the operations. In this context, robotic manipulators have been introduced in sanding and polishing applications. Inspired by the recent development in machine learning and robotics, this paper is focused on designing a system capable of estimating the surface roughness using only a force torque sensor integrated with a robotic manipulator that performs the sanding of fiberglass panels. We present an investigation into the usage of convolution neural networks on the force-torque data to produce a quantitative estimation of surface roughness. To validate the results obtained a profilometer is used to gather pre- and post-operation data. The establishment of a relationship between measured force data and post-operation surface roughness will be used to develop

a prediction of the surface quality for sanding operation using robotic manipulators. This project intents to act as proof-of-concept that traditional robotic sensors, can be used beyond their original scope, minimize the complexity of robotic systems integrated into manufacturing processes.

Keywords: robotics, neural networks, fiberglass panels, force-torque sensor, roughness

1 Introduction

In the composite materials industry, finishing operations such as sanding, polishing or trimming play an important role in the manufacturing process. These operations are primarily human-worker driven and require extensive knowledge and understanding of the process. As these tasks are purely qualitatively driven, based on worker's experience, they are dificult to automate, hence requiring machine-driven systems to determine satisfactory part completion. In the past years, robotic systems have been equipped with sanding tools and have been tele-operated [1] to perform finishing operations. The research started focusing towards automating the processes, developing control and planning architectures for robotic system performing sanding and polishing operations, based primarily on the geometry of the part. In these cases, the task was predetermined without considering task completion or the quality of the work [2, 3], the robotic system still relying on human operators to decide when the task has been completed.

Surface roughness is a common metric to assess the quality of a product [4]. For polymer composites, surface characteristics are especially important for applications where surface preparation is required after manufacturing for painting or bonding [5–7]. In the past years, various strategies have been developed to predict roughness for various types of materials and fabrication processes. Notably, significant work has been done to estimate roughness through computational methods. In [8], an overview of various approaches to predict surface roughness in turning and milling tasks, and for the same application in [9], presents a correlation between the tool vibration and the surface profile. A human study was presented in [10], which shows the correlation of the friction and force variation in the subjective determination of roughness through touch. Inspired by this method, an approach for correlating the finishing forces and the surface quality was established for magnetorheological abrasive flow finishing in [11], while a robotic system was used in [12] to estimate the contact forces based on part roughness. Nevertheless, most applications require special sensors and tooling [13, 14] to collect the data necessary for surface roughness estimation. Integrating such tooling and sensors into robotic systems can be time-consuming, expensive, and sometimes, not feasible if the robot is an off-the-shelf system.

Most robotic systems involved in any manipulation task are equipped with force-torque sensors that sense vibrations at the contact point. This represents useful information as vibrations could be used for surface roughness estimation as shown in [4]. Using a sensor that is already integrated with the robotic system can enable the robot to estimate the surface roughness of a part, and it would allow the realization of a feedback system that can be used to enable fully autonomous sanding or polishing without the need for human input. Furthermore, it would allow the creation of a simulation environment where various manufacturing strategies can be evaluated before being applied in practice.

The work presented here is focused on analyzing the data provided by force/torque sensors integrated with a robotic manipulator to predict surface roughness of glass fiber (GF)/epoxy laminates manufactured by vacuum-assisted resin infusion (VARI). Large composite parts requiring post-processing operations (i.e., sanding, painting, bonding) are commonly fabricated by this method, including components for the energy, aerospace, transportation, and maritime industries [15, 16]. Furthermore, this paper evaluates the performance of various machine learning approaches using the force measurements from robotic manipulators to estimate the surface roughness in composite panels. One of the main contributions of this paper is to show that raw force data, recorded at low frequencies, coming from off-the shelf robotic systems can be used with standard machine learning techniques to generate information regarding the surface roughness of glass fiber components. Such measurements and prediction framework can be used during automation processes to ensure high quality parts, and no specific surface roughness sensors need to be integrated in the process.

The paper is structured as follows: Section 2 presents an overview of previous work done in the field, Section 3 discusses composite laminates manufacturing, the experimental set-up, and the methodology for data collection, Section 4 discusses the data-driven approaches used in this work, Section 5 presents the estimation of the surface roughness, and Section 6 discusses the conclusions and future research avenues.

2 Related work

Autonomous finishing operations have been explored for several decades, both in research and industry. In [17], a robotic die polishing system was proposed, which used perception sensors. Furthermore, machine learning approaches were used to identify the texture of the environment and to identify the direction in which the polishing tool needs to act. In [18], a 5-axis polishing machine was introduced, capable of improving the surface quality of sculptured die surfaces using acoustic emission sensors to detect changes of the polishing status. In [19], the development of an autonomous sanding robot was presented. The robot was able to autonomously perform sanding operations on an unknown object without human intervention, using approaches such as impedance control and perception systems based on structured light.

One method to achieve uniform surface sanding or polishing using autonomous systems is to implement capability to evaluate and understand the surface characteristics by means of roughness estimation. Several works have focused on the design of modeling approaches to estimate the surface roughness. In [20], a prediction model that correlates material removal with applied pressure was developed based on elastic and plastic contact theory. In [8], both an analytical model and a geometric simulation were used to predict the surface roughness of a machined surface. A review of approaches used to predict surface roughness is detailed in [21], highlighting the emergence of machine learning approaches. In [22], surface roughness estimation for molds was presented using a three-layer artificial neural networks (ANN). The approach took into account the hardness, grit, pressure, tool speed, feed rate, polishing time, and prior surface roughness. In [23], it was found that neural networks can be used to effectively estimate surface roughness in computer numerical control (CNC) processes. Cutting speed, feed rate, and depth of cut were known input variables in the model. The authors found that accelerometer data was suficient to obtain usable information to predict surface roughness. While contact force is a factor in polishing quality, constant contact stress between the tool and part being polished is what determines the quality of a polished part. In [24], the authors developed a model for the contact stress between the polishing tool and the part, which allowed analysis of the contact stress during the operation. In [25], it was found that there is a relationship between material removal rate and vibration power input in a pitch polishing process.

Several papers in the literature have explored the topic of modeling finishing operations in the context of complex materials and geometries. In [26], an automatic polishing process for complex geometries was studied and resulted in a modeled surface roughness. The authors of [27] proposed a process for modeling and implementing robotic polishing operations in mold manufacturing. Xian et al. [28] studied the issue of vibration in the polishing process of a turbine blade with an abrasive cloth wheel. The authors established a method for analyzing the vibration characteristics of a polishing process in the frequency domain. Huang et al. [29] proposed an in-process monitoring system to predict surface roughness, and used this information as online input to a control system. Similarly, Bagaric et al. [14] developed a robotic sanding cell for thin-walled structures, equipped with a force control unit, and in-situ vibration, acoustic emission, and sound sensors, as well as an infrared camera and an optical sensor for roughness measurement. In [30], a surface roughness estimation method is presented based on frequency analysis for achieving smart sanding of wood panels through design of robust control systems. In [31], fast Fourier transform (FFT) data was used to predict roughness and to determine when to complete a robot-assisted polishing operation. The integration of FFT data into predictive roughness models was explored in [4], where the ability of three different predictive models to estimate roughness using vibration data was analyzed. It was concluded that out of one-dimensional convolution neural network (CNN), Fast Fourier Transform Deep Neural Network (FFTDNN),

and Fast Fourier Transform Long Short Term Memory Network (FFTLSTM), the CNN and FFTLSTM models produced similar and acceptable predictions. Vibration data, together with thermocouples, infrared temperature sensors, and accelerometers, were used in [32] to train a data-driven modeling approach to estimate surface roughness in additive manufacturing. In [33], prediction of surface quality of special-shaped stones by robotic grinding leveraged a combination of support vector machine models based on improved whale optimization algorithm. The input data used consisted of spindle speed, feed speed, cutting depth, and cutting width, while surface roughness measurements obtained with a roughness meter were used as outputs.

In this work, we propose to extend the studies presented above by focusing specifically on robust approaches for surface roughness estimation when robotic systems are used for sanding applications on polymer composite laminates using raw data. The work presented here investigates the benefits of using machine learning techniques with only force/torque data obtained at low sampling rates by the robotic system.

3 Experimental set-up

3.1 Composite laminates manufacturing

GF/epoxy laminates were used in this study. Saertex stitched biaxial glass fiber fabric (830 gsm areal density) was purchased from FiberGlast (Brookville, OH, USA). The laminates were manufactured by vacuum-assisted resin infusion (VARI) with System 4500 epoxy (FiberGlast), as illustrated in Fig. 1. An aluminum plate was used as a mold and three layers of release agent (Loctite 700-NC) were applied to facilitate demolding after fabrication. The fabric plies were cut into 23 cm × 23 cm squares and placed on the plate in a $[\pm 45]_3$ layup. The fabric was covered with a peel ply layer (Econostitch®) and resin flow medium mesh (Airtech Resinflow), then sealed with a nylon vacuum bagging film (Airtech Wrightlon® WL5400) and tacky tape (Airtech AT200Y). The vacuum bag was connected to an epoxy resin pot on one end and to a vacuum pump on the other, with spiral wrap and polyethylene tubing. After full vacuum was achieved, the resin was allowed to flow into the vacuum bag and fabric layers until full impregnation was completed. The laminate was then cured at room temperature for 6 to 8 hours.

3.2 Robotic system and design of experiments

For data collection, a robotic sanding setup, seen in Fig. 2, was used, combining a UR5e manipulator (Universal Robotics) and a Dremel Fortiflex orbital sander attached to the end-effector using a custom-made bracket.

A force-torque sensor was integrated in the end-effector of the robotic system, capable of recording the forces applied in the X, Y, Z directions of the end-effector. The sander speed was set to 23,000 RPM for each test, as recommended per manufacturer specifications. The sandpaper diameter was

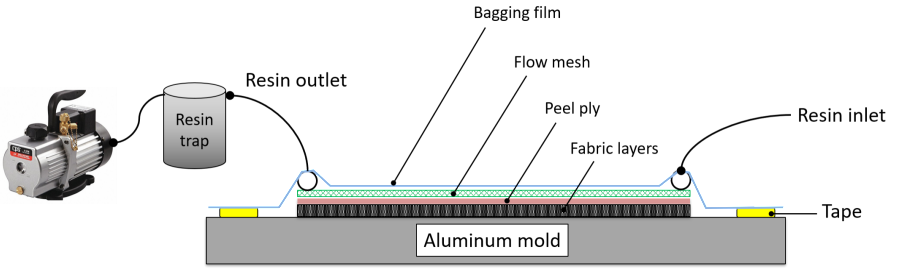

Fig. 1: Schematic of VARI setup to fabricate GF/epoxy laminates (pump from Grainger).

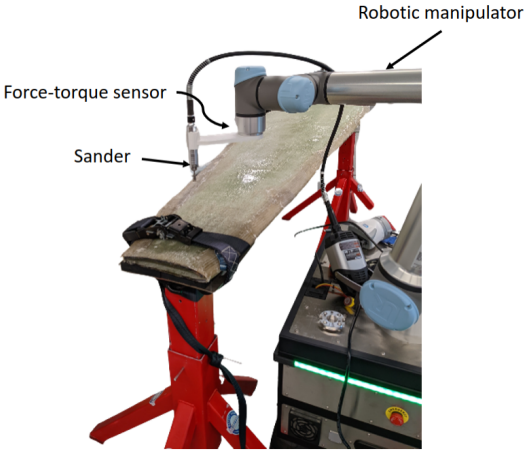

Fig. 2: Robotic sander system performing sanding on a small-scale GF/epoxy wind blade (2 meters in length).

25.4 mm and the grit size was 240. The sandpaper was attached to the bottom of the sanding tool. The robot was programmed to apply 2 N force in the Z direction, 0 N in the Y direction, and 0 N in the X direction during sanding. The force sensor was recorded using the UR5e's Real Time Data Exchange network protocol at 100 Hz (maximum operating frequency of the system). The data was collected by sanding 50 different areas on the GF/epoxy panels, each area being sanded for 10 seconds in a single pass.

4 Predictive roughness estimation

In this section, we present the benefit of machine learning techniques to estimate the roughness of GF/epoxy samples, as regression problems, by leveraging the information collected during sanding with the force-torque sensor placed at the end-effector of the manipulator.

4.1 Convolution Neural Networks

Here, a brief overview of the general structure of a CNN is presented to highlight the mechanism underlying its success. A CNN is a type of multi-layer neural network that has been extensively used in image processing applications, such as image recognition and identification [34]. Recently, advancements in the CNN structures have enabled such architectures to be used for multidimensional data classification and time series forecasting. It generally consists of layers like convolution, pooling, and fully connected layers. CNNs perform linear operations where the input is multiplied by a set of weights. Filters are specially designed to extract specific features from the input data. In a CNN, different features are determined by applying many filters in parallel. More features are obtained by adopting the filters to not only the input data, but also, to feature matrices obtained by filtering the inputs. To increase the non-linearity of the CNN, after the convolution process is completed, rectified linear units (ReLUs) can be used together with maximum functions. To solve the down-sampling problem, using the pooling layer, feature maps with fewer features and lower resolution are created. The pooling layer can also be applied more than once. Frequently used pooling operations are average pooling and maximum pooling. After the pooling is completed, its output is usually converted to one-dimensional data with the flatten layer and is transferred to the fully connected layer. At this stage, each activation function is interconnected and enables the extraction of high-level features from the data. At the end of this process, classification can be done with a soft − max layer or forecasting can be done with a regression layer.

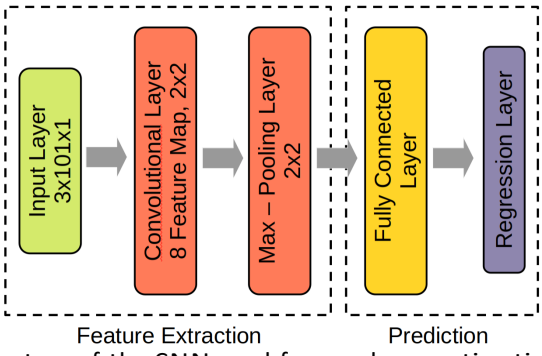

Fig. 3: The structure of the CNN used for roughness estimation in this study.

The CNN used for the proposed work, shown in Fig. 3, has one sequential input layer, one 2D convolution layer, an activation layer (hyperbolic tangent, tanh), a maximum pooling layer, a dropout layer, a fully connected layer, and a regression layer. The hyperparameters chosen are eight filters with 3×41 size each, a 0.003 learning rate, 0.35 dropout rate, and 2 strides. The input to the network is the three channels force data (X, Y, Z - axes) and the output is

the predicted roughness value. Extracting features from the input data before the input layer generally increases the performance of the network, however, in this case, it is unnecessary for the force data due to the CNN's powerful feature extraction capability.

4.2 Long Short-Term Memory Network

Recurrent Neural Networks (RNNs) are a class of neural networks which can learn time series and sequential data. They have gained recognition in natural language processing and time series forecasting [35]. Some special types of RNNs include Long Short-Term Memory (LSTM) networks, Gated Recurrent Networkss (GRUs), and bidirectional models of LSTMs and GRUs.

LSTM has the advantage that it can learn long-term dependencies, being developed to solve the vanishing gradient problem. This network structure works by ignoring "bad" data and learning only from the useful data. The general structure of an LSTM network is given in Fig. 4 and consists of three layers: forget gate, input gate, and output gate. In the input, the information to be extracted from the cell-state is selected using a sigmoid function by the forget gate. Then, by the input gate, new information is created to add to the cell-state using i_t and c'_t functions, as shown in Equation (1). The sigmoid function decides whether to add new information to the current data or not. The tanh function creates the values to be added to cell-state using the input data. In the output gate, the output data is calculated by Equation (2).

$$\begin{aligned} i_t &= \sigma(W_i \cdot h_{t-1}, x_t + b_i)\, c_t \\ &=, \tanh(W_C \cdot [h_{t-1}, x_t] + b_c) \\ o_t &= \sigma(W_o \cdot h_{t-1}, x_t + b_o) \end{aligned} \tag{1}$$

$$h_t = o_t \cdot \tanh(c_t) \tag{2}$$

where h_t is the hidden state of the current timestamp and x_t is the current input, while b_i, b_c, and b_o are the biases, W_i, W_c and W_o are the weight matrices of the input, current state, and output, respectively, and subscript $t-1$ refers to the previous timestamp.

The sigmoid function decides whether the relevant data should pass to the output or not. In this work, the LSTM structure consists of two LSTM layers with 120 and 80 hidden units, a dropout layer (rate of 0.3), a fully connected layer, and a regression layer. The inputs to the LSTM are the three channel force data and the output is the predicted roughness value. The LSTM structure used for the proposed work is shown in Fig. 5

4.3 Hybrid Neural Network

Due to the capabilities of extracting the features from raw force data by a CNN, such an approach can be coupled with the LSTM structure for prediction of surface roughness.

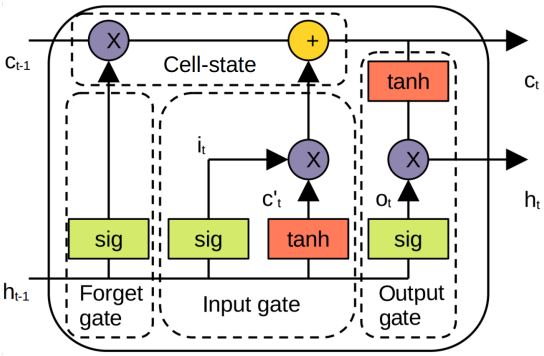

Fig. 4: The general structure of LSTM.

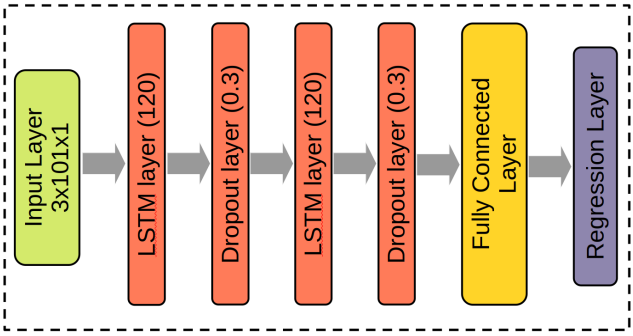

Fig. 5: The structure of the LSTM network used for surface roughness estimation.

A hybrid network was designed by using 2D CNN and LSTM networks to combine their capabilities in feature extraction for time series. The structure of the hybrid CNN-LSTM network is given in Fig. 6. The inputs of the network is the three channel force data and the output is the roughness values. The hybrid CNN-LSTM model has an input layer, a sequence folding layer, a 2D convolution layer, an activation layer (tanh), a maximum pooling layer, a dropout layer (with rate 0.03), a sequence unfolding layer, a flatten layer, a LSTM layer with 20 hidden units, a dropout layer (with rate of 0.3), a fully connected layer, and a regression layer. The hyperparameters of the hybrid network are the same as the CNN model, except for the dropout rate, chosen as 0.3.

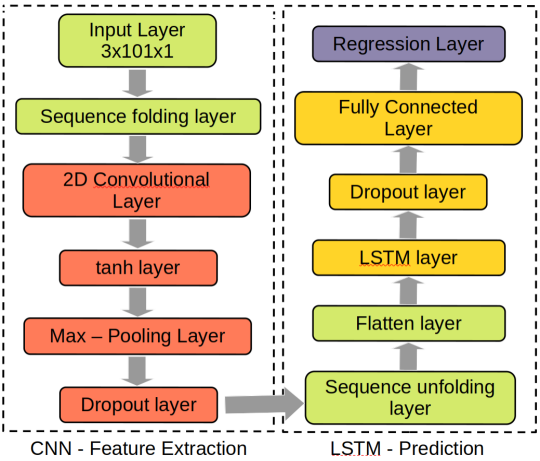

Fig. 6: The structure of the hybrid CNN-LSTM network used for surface roughness estimation.

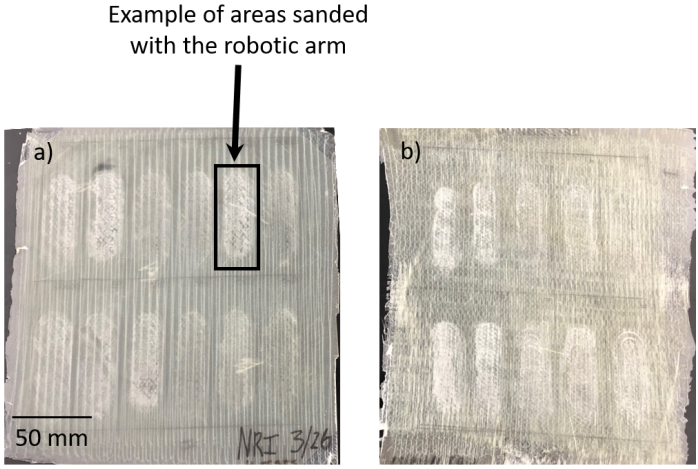

Fig. 7: Example of GF/epoxy samples sanded with the robotic manipulator: (a) shows a laminate divided in 12 sections, while (b) is divided into 10 sections. Each section represents a sanded area where roughness measurements were acquired.

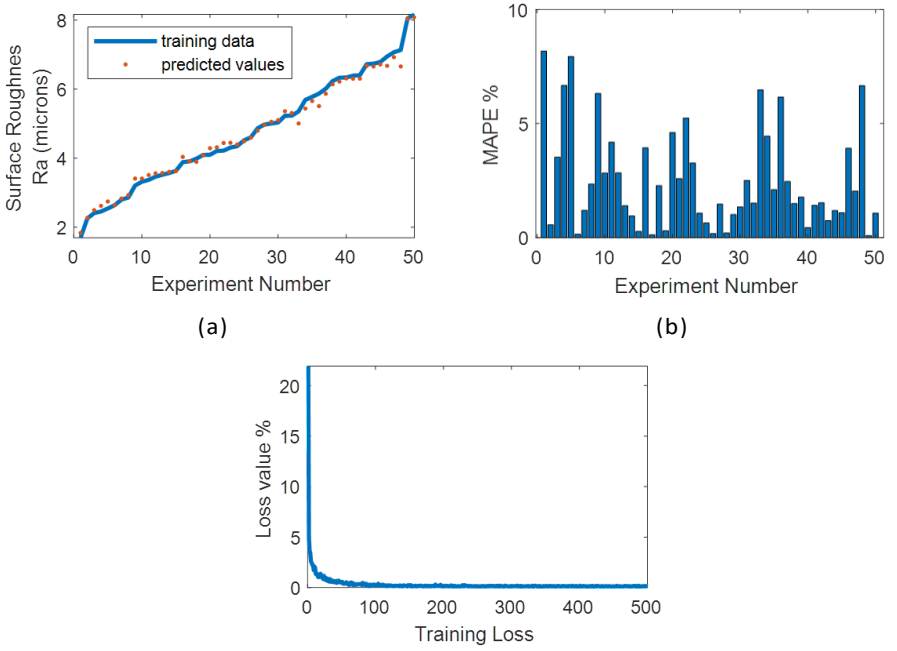

Fig. 8: Training results of the CNN: a) Distribution of predicted R_a values; b) Error graph of the predicted R_a values; and c) Loss function output during training.

5 Results

5.1 Datasets Preparation

A total of 50 GF/epoxy specimens were sanded with the system presented in Section 3 and raw force data was collected during the sanding process. A few examples of manufactured laminates sanded by the robotic system are shown in Fig. 7. The force sensor acquired three-axis vibration data (in the X, Y, Z -axes), with 100 samples per second for each axis, and a total of 300 data points collected during each test. Data collected at a higher sampling rate would result in a more detailed understanding regarding the behavior of the system, therefore, better training and more accurate predictions could be obtained. However, the robotic system used in this research works at a maximum frequency of 100 Hz. This work aims to demonstrate that robotic systems operating at low frequencies can be used in manufacturing applications. Hence, it is preferable to use the data collected by the robotic system rather than introducing an additional higher resolution sensor, which would be out of the scope of this study.

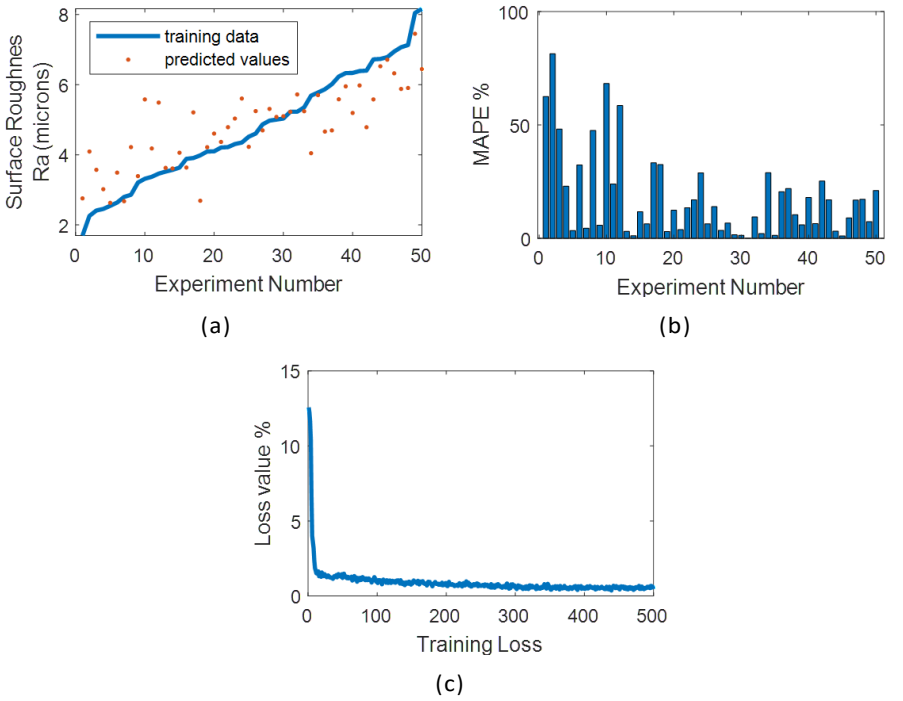

Fig. 9: Training results of LSTM: a) Distribution of predicted R_a values; b) Error graph of the predicted R_a values; and c) Loss function output during training.

To validate the roughness of the material, a portable surface roughness tester (Mitutoyo Surftest SJ-210) was used to obtain the ground truth roughness measurements before and after sanding. The average roughness (R_a in µm) was recorded over the same area the robotic sanding was performed. The inputs for the CNN, LSTM, and hybrid neural networks were obtained from the force sensor measurements and the outputs for all networks were the R_a values from the roughness tester. The problem to be solved by these networks was posed as a regression problem, hence the data gathered was organized in ascending order based on the roughness measurement values.

The performance of the approaches discussed in Section 4 was evaluated in three different ways. A first approach was considered by analyzing and visualizing the loss value graphs, Mean Absolute Percentage Error (MAPE) graphs, and analyze the Root Mean Square Errors (RMSE) values when the full dataset was used at the training stage. This step is needed to confirm that the network can learn from the dataset used in the study. A second evaluation focused on dividing the dataset into training and testing specimens, using 90% data points for training and 10% for testing. This stage is important to confirm that the trained network can predict the test data. Lastly, cross-validation

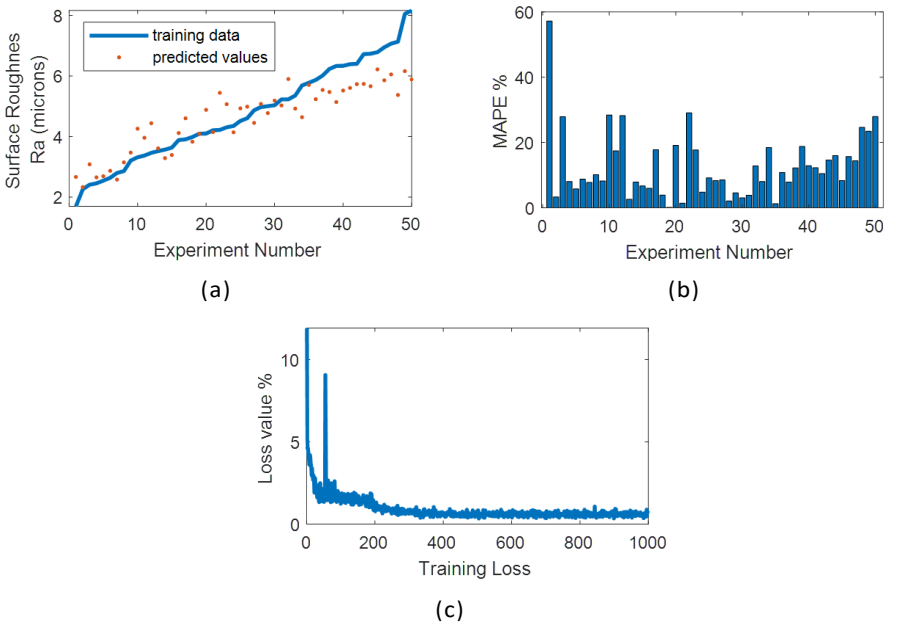

Fig. 10: Training results of CNN-LSTM: a) Distribution of predicted R_a values; b) Error graph of the predicted R_a values; and c) Loss function output during training.

was used to evaluate the performance of the system on all datasets. All hyper parameters used in this work for the CNN, LSTM, and hybrid CNN-LSTM, including training parameters, are given in Table 1.

5.2 Experimental Results

Evaluation during training: The performance of the three models during the training process was evaluated using all the data points available. The predicted value graphs are given in Fig. 8(a), Fig. 9(a), and Fig. 10(a) for the CNN, LSTM, and hybrid approaches, respectively. The blue line shows the measured roughness values of the dataset (ground truth), and the red dots are the predicted roughness values by the respective networks. Qualitatively, it can be seen that both LSTM and hybrid approach have similar accuracy, with the LSTM shows slightly better performance. This can also be analyzed by investigating the performance of the loss function.

The loss function shows the difference between the output values of the trained network and the ground truth values. This function gives insight into how well the data has been learned. Its output is expected to converge toward zero. Loss function graphs of the CNN, LSTM, and hybrid networks are given in Fig. 8(c), Fig. 9(c), and Fig. 10(c). While all three models converge to zero and have acceptable convergence values, the CNN and LSTM networks have a more

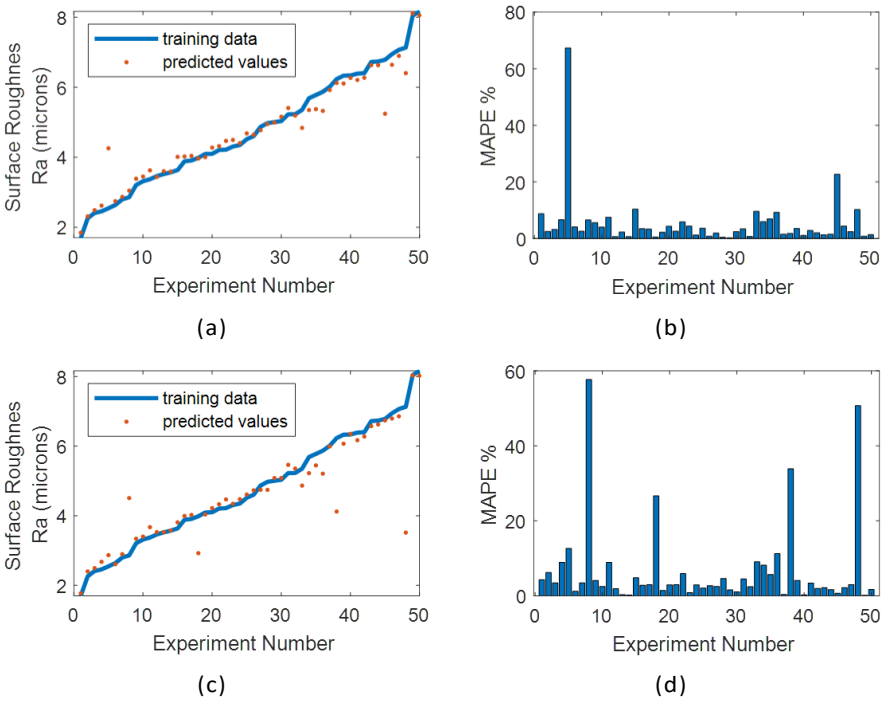

Fig. 11: Training results of CNN for selected intervals: Test Set 3 and Test Set 5. (a) Distributions of predicted values when Test Set 3 is used; (c) Distributions of predicted values when Test Set 5 is used; (b) Error graphs of the predicted Ra values when Test Set 3 is used; (d) Error graphs of the predicted Ra values when Test Set 5 is used.

	Hybrid CNN-LSTM	LSTM	CNN
Input size	[3 101 1]	3	[3 101 1]
2D Convolution layer	FS = 8	-	FS = 8
Activation layer	tanh	-	tanh
Max. pooling layer	FS = 2, Stride=2	-	FS = 2, Stride=2
Number of neurons (LSTM)	20	120/80	-
Dropout layer	0.03/0.3	0.3/0.3	0.35
Fully connected layer	Number of outputs = 1		
Mini batch size	64		
Optimizer	Adam		
Max. epochs	500		
Initial learning rate	0.006		
Shufle	Every epoch		

Table 1: Hyper parameters for CNN-LSTM, LSTM, and CNN networks, including training parameters. FS refers to filter size.

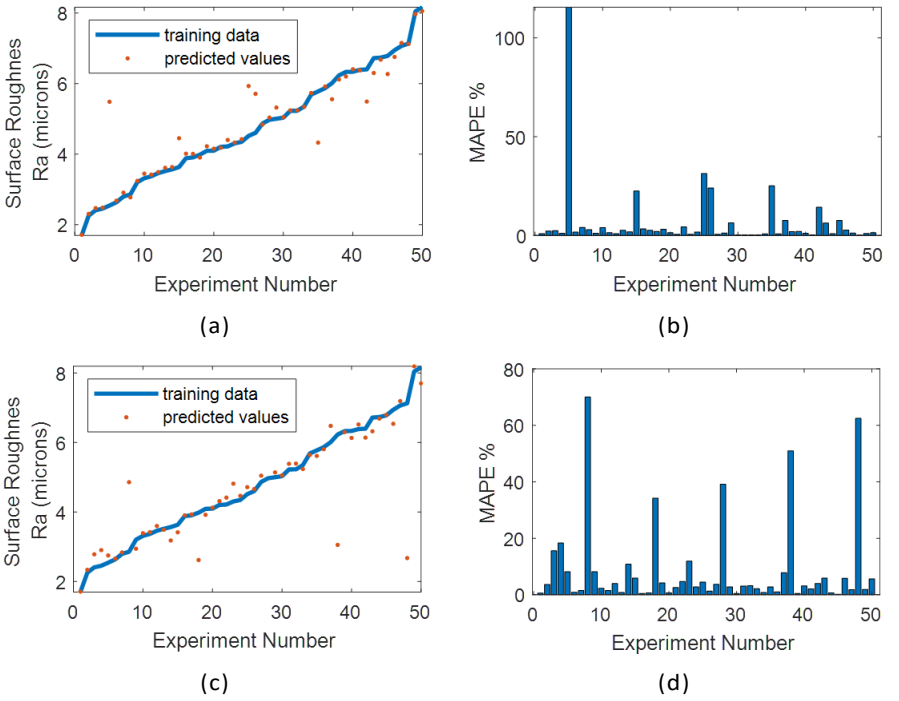

Fig. 12: Training results of LSTM for selected intervals: Test Set 3 and Test Set 5. (a) Distributions of predicted values when Test Set 3 is used; (c) Distributions of predicted values when Test Set 5 is used; (b) Error graphs of the predicted Ra values when Test Set 3 is used; (d) Error graphs of the predicted Ra values when Test Set 5 is used.

stable behavior, while the hybrid approach presents a more oscillatory behavior over the iterations. The CNN shows good convergence performance during training, as demonstrated quantitatively in the following paragraph. The Mean Absolute Percentage Error (MAPE) and Root Mean Square Errors (RMSE) calculations were used to compare the estimation capabilities of the networks. The formulations of these metrics are given in Equation (3) and Equation (4).

$$MAPE = \frac{1}{n}\sum_{j=1}^{n}\frac{y_j - x_j}{y_j} \times 100 \tag{3}$$

$$RMSE = \sqrt{\frac{1}{n}\sum_{j=1}^{n}(y_j - x_j)^2} \tag{4}$$

where y_j represents the prediction obtained from the corresponding network for the j-th sample, x_j represents the ground truth measurement obtained with the roughness tester for the same sample. The results are presented in Table 2, while the MAPE graph is presented in Fig. 8(b), Fig. 9(b), and Fig. 10(b).

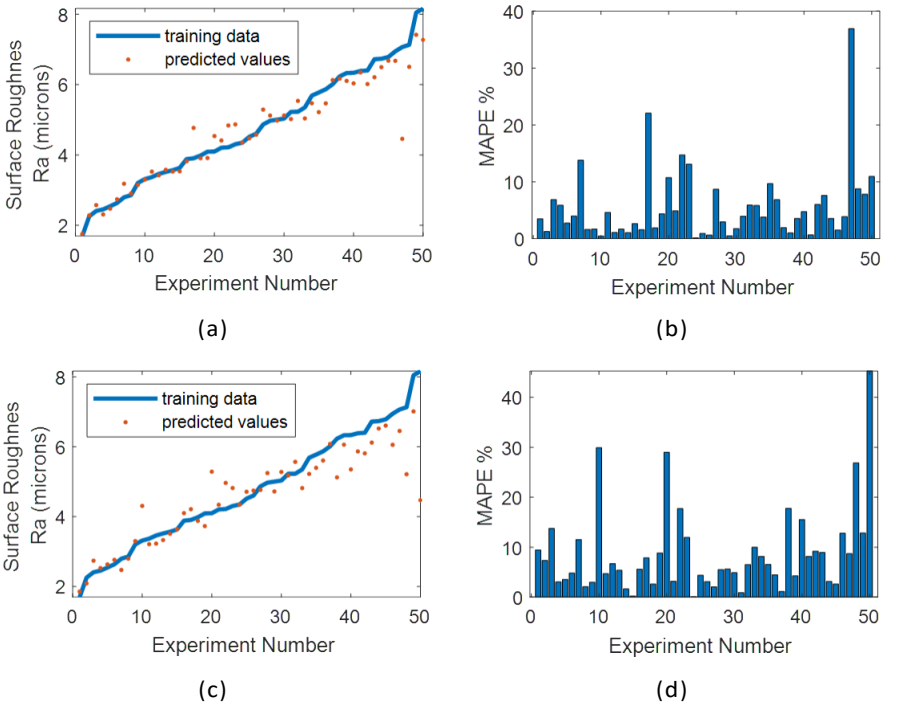

Fig. 13: Training results of CNN-LSTM for selected intervals: Test Set 3 and Test Set 5. (a) Distributions of predicted values when Test Set 3 is used; (c) Distributions of predicted values when Test Set 5 is used; (b) Error graphs of the predicted Ra values when Test Set 3 is used; (d) Error graphs of the predicted Ra values when Test Set 5 is used.

	CNN	LSTM	Hybrid CNN - LSTM
RMSE	0.107	0.455	0.814
MAPE [%]	2.53	18.04	12.77

Table 2: RMSE and MAPE for all three networks when all data points were used during training.

These results indicate an average MAPE over 10% for the hybrid approach, and over 18% for the LSTM. During these tests, it was observed that the LSTM network performs similarly to the CNN-LSTM, while CNN can overfit the data, as seen on Fig. 14. The validation frequency is set for every 10 iterations, and it is observed that the test and validation errors are high while the training error is low, which means that the network is overfitting.

Training-Testing Evaluation: The results of the above evaluation showed that all networks can be trained using the dataset, but do not provide guidance about the prediction performance. A second evaluation is needed to see if the

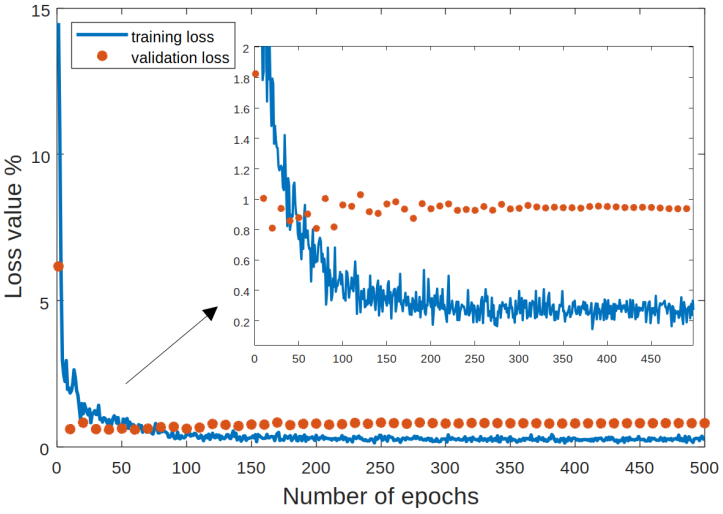

Fig. 14: Training-validation graph of the CNN network; zoomed image shows more clearly the differences between the training loss and validation loss

networks can predict the test data that is not used in the training process. To properly evaluate the prediction performance of the networks, the available dataset is divided into two groups: training and testing datasets. Testing is performed with data not used for training. Due to the limited dataset, the performance was examined by separating the data in a 90% – 10% training-testing ratio.

To obtain meaningful results, it was ensured that the testing data covered all ranges of surface roughness measured. To achieve this, the data was grouped as follows. Initially, the complete dataset was sorted from the smallest to the largest value according to their R_a values. The dataset was further divided into five sections, based on the R_a values, where each section contained 10 samples. The division of these sections is presented in Table 3. The first and the fifth sections contain the low-range R_a values and high-range R_a values respectively, while the other three sections contain the medium-range R_a values. The next step was to randomly select the testing data such that for all testing groups, samples were taken from each of the subsections described above. Hence, it was ensured that each testing dataset contained data from all ranges of the collected roughness values. All ten testing sets were used to evaluate the performance of the system, as seen in Table 3. When one of these testing sets was used for testing, it was not used for training.

The results for the training performance of the CNN, LSTM, and hybrid approached are seen in Fig. 11, Fig. 12, and Fig. 13, respectively, for the case when Set 3 and Set 5 were used for testing. The LSTM presents large prediction errors based on the qualitative results and MAPE metrics. The LSTM overfits data at the end of the training process, as shown in Fig. 12. This is an expected result for LSTM because it cannot extract features when little data is available.

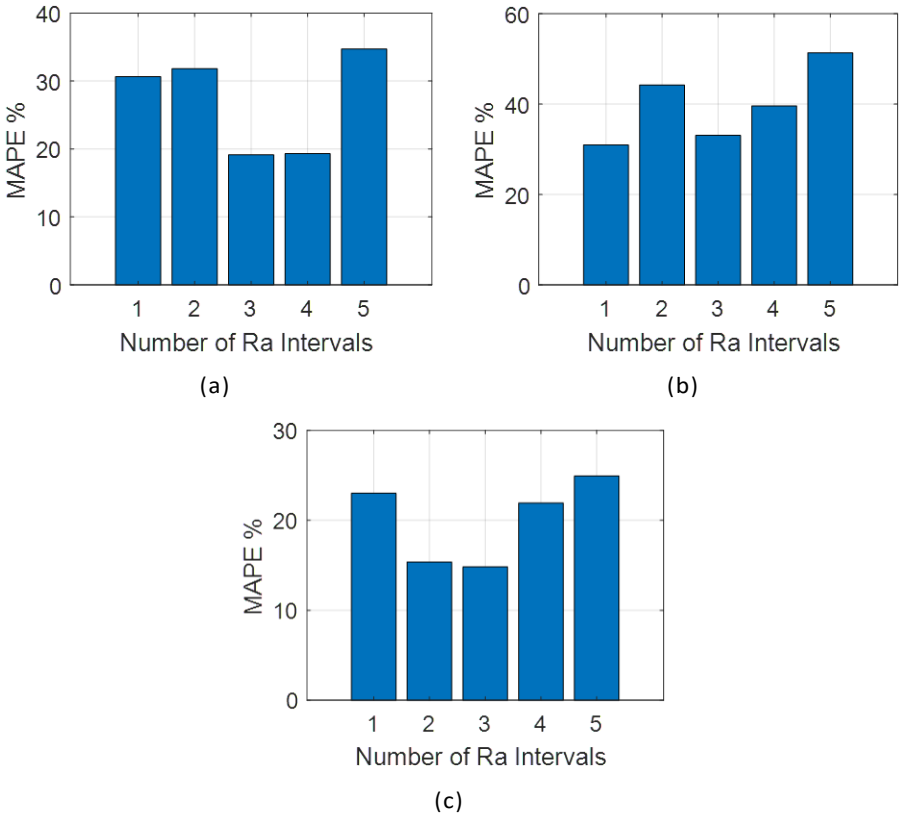

Fig. 15: Cross-validation results for (a) CNN, (b) LSTM, and (c) CNN-LSTM networks.

The CNN presents good performance for Test Set 3, with lower performance for Test Set 5, while hybrid CNN-LSTM has the lowest mean error values for both datasets. These results are as expected due to the large variability in the datasets. To ensure that the performance of machine learning approaches are viable for such datasets, cross-validation is presented in the next paragraphs.

Cross-validation: The training-testing evaluation shows that the proposed networks can predict the test data. To understand the capabilities of the network to avoid overfitting and estimate the capabilities of the model on new data, cross-validation is performed to see the overall prediction performance of the trained models. Five different testing datasets were selected randomly, as presented in Table 4. For each validation dataset, the remaining 45 data are used for training.

For all the testing sets, the MAPE values were calculated for each of the testing sets and averaged. This process was repeated for the CNN, LSTM, and hybrid networks, shown in Fig. 15. For all testing cases, hybrid CNN-LSTM has the lowest MAPE values between 14.83% – 24.91%, with an average

Range	Lower	Medium			Higher
Number	1-10	11-20	21-30	31-40	41-50
Set 1	1.697	3.372	4.207	5.227	6.389
Set 2	2.257	3.462	4.219	5.229	6.401
Set 3	2.410	3.520	4.306	5.353	6.721
Set 4	2.456	3.569	4.349	5.688	6.735
Set 5	2.544	3.634	4.516	5.776	6.785
Set 6	2.638	3.885	4.605	5.869	6.945
Set 7	2.798	3.908	4.867	6.013	7.068
Set 8	2.859	3.985	4.975	6.232	7.131
Set 9	3.207	4.094	5.004	6.330	8.046
Set 10	3.317	4.099	5.034	6.336	8.165

Table 3: Rearranged training data R_a values.

Testing Set Number	Samples
3	(3, 13, 23, 33, 43)
4	(4, 14, 24, 34, 44)
5	(5, 15, 25, 35, 45)
7	(7, 17, 27, 37, 47)
8	(8, 18, 28, 38, 48)

Table 4: Testing sets considered for cross-validation based on sample number.

value of 20%. CNN has MAPE values between 19.14% and 37.71%, with an average of 27.12%. The LSTM-based model has MAPE values between 30.97% and 51.37%, with an average of 39.86%, showing the lowest performance out of all the networks tested. Furthermore, the CNN and hybrid CNN-LSTM models have better prediction results for mid-range R_a values. The LSTM presents poorer results, as high frequency is challenging for feature extraction without data preprocessing, and some characteristic data can be affected by environmental noise at the lower range. Overall, the cross-correlation results show that the CNN-LSTM model can be used for accurate surface roughness estimation in sanding processes.

6 Conclusions

In this paper, we demonstrated that using force-torque measurements recorded using a robotic manipulator performing sanding operations can be used to estimate surface roughness in polymer composite laminates. Furthermore, the design and evaluation of deep learning networks for surface roughness prediction using vibration data recorded during the sanding process were presented. A CNN, LSTM, and hybrid CNN-LSTM networks were used and evaluated based on training and prediction performances. All three models displayed good training performances, although the CNN-LSTM based approach had the best prediction performance when comparing the cross-validation outcomes. CNN had the second-best prediction performance owing to its feature extraction capability. The LSTM network had poorer results, due to the nature of LSTM,

which cannot handle raw data. However, LSTM improved the CNN network in the hybrid configuration to achieve better results by combining the feature-extracting capability of CNNs and the time series learning ability of LSTM. As a result, prediction results of the CNN-LSTM model had MAPE values between 14.83% and 24.91%. Hence, the CNN-LSTM based surface roughness framework leads to suficient predictions and may be helpful during sanding processes. As future work, a real-time surface roughness prediction system based on the CNN-LSTM model will be designed by also collecting a larger dataset to improve accuracy. Furthermore, other learning approaches, such as spiked neural networks, will be designed to enable reliable estimations when limited datasets are available.

Declarations

Funding

The authors would like to acknowledge financial support from NSF #2024795, "NRI: FND: Collaborative Mobile Manufacturing in Uncertain Scenarios".

Competing Interests

The authors have no relevant financial or non-financial interests to disclose.

Author Contributions

All authors contributed to the paper's conception and design. Algorithm implementation was performed by Huseyin Oktay Erkol, data collection and study configuration was performed by Manuel Bailey, material preparation was performed by Dr. Genevieve Palardy, and data analysis was performed Huseyin Oktay Erkol and Corina Barbalata. The first draft of the manuscript was written by Manuel Bailey, Huseyin Oktay Erkol, and Corina Barbalata, and all authors commented on previous versions of the manuscript. All authors read and approved the final manuscript.

References

[1] Höglund T, Alander J, Mantere T. A survey of telerobotic surface finishing. Open Engineering. 2018;8(1):156–161.

[2] García A, Gracia L, Solanes JE, Girbés-Juan V, Perez-Vidal C, Tornero J. Robotic assistance for industrial sanding with a smooth approach to the surface and boundary constraints. Computers & Industrial Engineering. 2021;158:107366.

[3] Kharidege A, Ting DT, Yajun Z. A practical approach for automated polishing system of free-form surface path generation based on industrial arm

robot. The International Journal of Advanced Manufacturing Technology. 2017;93(9):3921–3934.

[4] Lin WJ, Lo SH, Young HT, Hung CL. Evaluation of deep learning neural networks for surface roughness prediction using vibration signal analysis. Applied Sciences. 2019;9(7):1462.

[5] Kwon DJ, Kim JH, Kim YJ, Kim JJ, Park SM, Kwon IJ, et al. Comparison of interfacial adhesion of hybrid materials of aluminum/carbon fiber reinforced epoxy composites with different surface roughness. Composites Part B: Engineering. 2019;170:11–18.

[6] Li W, Sang L, Jian X, Wang J. Influence of sanding and plasma treatment on shear bond strength of 3D-printed PEI, PEEK and PEEK/CF. International Journal of Adhesion and Adhesives. 2020;100:102614.

[7] Palardy G, Hubert P, Haider M, Lessard L. Optimization of RTM processing parameters for Class A surface finish. Composites Part B: Engineering. 2008;39(7-8):1280–1286.

[8] Meijer A, Bergmann JA, Krebs E, Biermann D, Wiederkehr P. Analytical and simulation-based prediction of surface roughness for micromilling hardened HSS. Journal of Manufacturing and Materials Processing. 2019;3(3):70.

[9] Abouelatta O, Madl J. Surface roughness prediction based on cutting parameters and tool vibrations in turning operations. Journal of materials processing technology. 2001;118(1-3):269–277.

[10] Smith AM, Chapman CE, Deslandes M, Langlais JS, Thibodeau MP. Role of friction and tangential force variation in the subjective scaling of tactile roughness. Experimental brain research. 2002;144(2):211–223.

[11] Jayant, Jain V. Analysis of finishing forces and surface finish during magnetorheological abrasive flow finishing of asymmetric workpieces. Journal of Micromanufacturing. 2019;2(2):133–151.

[12] Parsons DF, Walsh RB, Craig VS. Surface forces: Surface roughness in theory and experiment. The Journal of chemical physics. 2014;140(16):164701.

[13] Creath K, Wyant JC. Absolute measurement of surface roughness. Applied optics. 1990;29(26):3823–3827.

[14] Bagaric D, Staroveski T, Klaic M, Ciglar D. ONLINE MULTI–SENSOR PROCESS MONITORING DURING ROBOTIC SANDING OF THIN-WALLED STRUCTURES. Annals of DAAAM & Proceedings. 2022;33.

[15] Vasanthanathan A, Navin Kumar C. Fabrication of aluminum honeycomb cored carbon fabric/epoxy composite sandwich structures via vacuum assisted resin infusion technique. Polymer Composites. 2022;43(3):1407 – 1420.

[16] Murray RE, Penumadu D, Cousins D, Beach R, Snowberg D, Berry D, et al. Manufacturing and Flexural Characterization of Infusion-Reacted Thermoplastic Wind Turbine Blade Subcomponents. Applied Composite Materials: An International Journal for the Science and Application of Composite Materials. 2019;26(3):945 – 961.

[17] Kuo RJ. A robotic die polishing system through fuzzy neural networks. Computers in Industry. 1997;32(3):273–280.

[18] Ahn J, Lee M, Jeong H, Kim S, Cho K. Intelligently automated polishing for high quality surface formation of sculptured die. Journal of Materials Processing Technology. 2002;130:339–344.

[19] Huo Y, Chen D, Li X, Li P, Liu YH. Development of an autonomous sanding robot with structured-light technology. In: 2019 IEEE/RSJ International Conference on Intelligent Robots and Systems (IROS). IEEE; 2019. p. 2855–2860.

[20] Zhang L, Tam H, Yuan C, Chen Y, Zhou Z. An investigation of material removal in polishing with fixed abrasives. Proceedings of the Institution of Mechanical Engineers, Part B: Journal of Engineering Manufacture. 2002;216(1):103–112.

[21] Benardos P, Vosniakos GC. Predicting surface roughness in machining: a review. International journal of machine tools and manufacture. 2003;43(8):833–844.

[22] Wang G, Zhou H, Wang Y, Yuan X. Modeling surface roughness based on artificial neural network in mould polishing process. In: 2014 IEEE International Conference on Mechatronics and Automation. IEEE; 2014. p. 799–804.

[23] Risbood K, Dixit U, Sahasrabudhe A. Prediction of surface roughness and dimensional deviation by measuring cutting forces and vibrations in turning process. Journal of Materials Processing Technology. 2003;132(1-3):203–214.

[24] Roswell A, Xi FJ, Liu G. Modelling and analysis of contact stress for automated polishing. International Journal of Machine Tools and Manufacture. 2006;46(3-4):424–435.

[25] Mainuddin M. Precision polishing dynamics: the influence of process vibrations on polishing results. The University of North Carolina at Charlotte; 2014.

[26] Tian F, Li Z, Lv C, Liu G. Polishing pressure investigations of robot automatic polishing on curved surfaces. The International Journal of Advanced Manufacturing Technology. 2016;87(1):639–646.

[27] Márquez J, Pérez J, Rıos J, Vizán A. Process modeling for robotic polishing. Journal of Materials Processing Technology. 2005;159(1):69–82.

[28] Xian C, Shi Y, Lin X, Liu D. Study on vibration characteristics of polishing rod for polishing aeroengine blade with abrasive cloth wheel. Mathematical Problems in Engineering. 2020;2020.

[29] Huang PTB. A neural networks-based in-process adaptive surface roughness control (NN-IASRC) system in end-milling operations. Iowa State University; 2002.

[30] Nguyen J, Bailey M, Carlucho I, Barbalata C. Robotic Manipulators Performing Smart Sanding Operation: A Vibration Approach. In: 2022 International Conference on Robotics and Automation (ICRA). IEEE; 2022. p. 2958–2964.

[31] De Agustina B, Marín MM, Teti R, Rubio EM. Analysis of force signals for the estimation of surface roughness during Robot-Assisted Polishing. Materials. 2018;11(8):1438.

[32] Li Z, Zhang Z, Shi J, Wu D. Prediction of surface roughness in extrusion-based additive manufacturing with machine learning. Robotics and Computer-Integrated Manufacturing. 2019;57:488–495.

[33] Yin F, Ji Q, Cun C. Data-Driven Modeling and Prediction Analysis for Surface Roughness of Special-Shaped Stone by Robotic Grinding. IEEE Access. 2022;10:67615–67629.

[34] Ozer I, Ozer Z, Findik O. Noise robust sound event classification with convolutional neural network. Neurocomputing. 2018;272:505–512.

[35] Sherstinsky A. Fundamentals of recurrent neural network (RNN) and long short-term memory (LSTM) network. Physica D: Nonlinear Phenomena. 2020;404:132306.